CrossMark

Hydrothermally grown of well-aligned ZnONRs: dependence of alignment ordering upon precursor concentration

Marjoni Imamora Ali Umar[1] · Fitri Yenni Naumar[1] · Muhamad Mat Salleh[2] · Akrajas Ali Umar[2]

Abstract

The well-aligned Zinc Oxide Nanorods (ZnONRs) arrays was obtained through a hydrothermal process at various precursor concentrations (PC) under a growth temperature of 90 °C for an hour. The effect of PC (0.02, 0.03, 0.04, 0.05, and 0.06 M which is denoted as K0.01–K0.06) to the structural, optical, and morfology (diameter, height, slope, and density) of ZnONRs were studied by using X-ray diffraction, UV–Vis spectroscopy, and field emission scanning electron microscopy (FESEM). As-synthesized ZnONRs exhibit an uniform growth direction along the [002] orientations with average diameters in the range of 40–90 nm. These nanorods showed a strong optical absorption peak centering at 367 nm, which is equivalent to optical energy band gap of ZnO 3.37 eV, confirming the formation of ZnONRs. The morfology of ZnONRs in term of diameter, height, slope, and density increases with the PC. The highest density of approximately 182 number/μm^{-2} with average slope of 6 degree (aligning percentage of $83 \pm 12\%$) was obtained at the PC of K0.04. It is interesting to find that the dye sensitized solar cell utilizing the sample K0.04 showed five times increasing in the power conversion efficiency as compared to that of device utilizing K0.02 sample.

1 Introduction

Research efforts to produce an extended and well-align of ZnO nanorods (ZnONRs) has been obtaining a continuous attention in the last few decades due to their unique electrical and optical properties [1]. Besides that, the ZnONRs is expected to further enhance their intrinsic property and make them as a potential material candidates for many applications, such as chemical and biology sensor, microelectronics devices, energy conversion and storage [2]. Previously, Tian and his co-worker have been successfully preparing the aligned ZnONRs by using a high-temperature vacuum deposition [3]. However, it usually requires a single-crystal substrate and applied in a high operating temperature, inferring it is an expensive method [4]. In addition, this method

is inappropriate for organics substrate for a microelectronic application. Similarly, Singh and his co-worker also report a facile method to produce well-aligned ZnONRs via a controlled thermal evaporation of Zn powder [5]. However, it also requires a high preparation's temperature and gas application (argon and oxygen) during the preparation process.

Recently, many approaches for preparing ZnONRs on the surface of the organic substrate at low temperature has been introduced and widely used. Such as through anodic aluminium oxide template electrochemical, and hydrothermal methods [6–14]. Among the available techniques, the hydrothermal methods is a very suitable to produce ZnONRs with high-density and well-aligned under a low temperature processing [6]. Since the property of ZnONRs, such as morphologies, compositions, and alignment, strongly depend on the synthesis protocol, particularly the precursor concentration, to control the synthetic condition may produce well-aligned ZNONRs on substrate surface. In this paper, we demonstrate the preparation of well-aligned ZnONRs by controlling the concentration of precursors during the growth process. A suitable condition that project the growth of high-density and well-aligned ZnONRs are obtained. The synthetic method and the mechanism for the growth of high-density and well-aligned ZnONRs will be discussed.

✉ Marjoni Imamora Ali Umar
marjoniimamora@iainbatusangkar.ac.id;
marjoniimamora@gmail.com

[1] Department of Physics Education, Faculty of Tarbiyah and Teaching (FTIK), Institut Agama Islam Negeri (IAIN) Batusangkar, Batusangkar 27213, West Sumatera, Indonesia

[2] Institute of Microengineering and Nanoelectronics (IMEN), Universiti Kebangsaan Malaysia, 43600 Bangi, Selangor, Malaysia

2 Experimental

In a typical procedure, we grouped the study into two simple steps, namely: preparation of ZnONRs, and fabrication a photovoltaic electrochemical cell. The detailed of each step will be explained as follows:

2.1 Preparation of ZnONRs

ZnONRs arrays were prepared on FTO on glass substrates which were pre-coated with ZnO nanoparticles seed using hydrothermal process. ZnO nanoparticles seeds were prepared by a sol–gel process using a reaction containing zinc acetate (Zn $(H_3COO)_2·H_2O$) (98%, Sigma-Aldrich) and DEA $(C_4H_{11}NO_2)$ (99%, Sigma-Aldrich) in ethanol. Thin film of ZnO nanoparticles seeds on FTO substrate were then prepared by a spin-coating method at 400 rpm for 30 s. The FTO substrate containing the ZnO nanoparticles seed was then subjected to an annealing process at 300 °C in air for an hour. The ZnONRs were grown up from the nanoparticles seed via a hydrothermal method in a growth solution containing equimolar zinc nitrate hexahydrate (99%, Sigma-Aldrich) and hexamethyl-tetramine (99%, Sigma-Aldrich) in DI water. The reaction was then carried out in an autoclave at 90 °C for 1 h. The detail of the ZnONRs preparation processes has been described elsewhere [15–17]. In this paper, the growth precursor concentration (PC) was varied from 0.02 to 0.06 M with sample's name denoted as K0.02, K0.03, K0.04, K0.05, and K0.06. All chemical reagents used in the experiment are of analytical grade and used without further purification.

2.2 Fabrication of photovoltaic electrochemical cell

The preparation of ZnONRs as the photovoltaic material has been described in the previous section. Platinum [18–20] have been used as a counter electrode to study the photovoltaic performance of dye-sensitized solar cell (DSSC). Platinum is prepared by using magnetron sputtering technique by using platinum pellet on FTO substrate at 2.5 kV for 2 min under vacuum. An electrolyte containing a redox couple of iodide/tri-iodide, i.e. a mixture of 0.5 M LiI, 0.05 M I_2 and 0.5 M tertbutyl pyridine in acetonitrile was used in this study [18, 19, 21–25]. The electrolyte was sandwiched between the ZnONRs structure and platinum as a counter electrode as shown in Fig. 1. The resultant cell was clamped each other using a paper clip and the photovoltaic performance of DSSC cell was studied by using an AM 1.5 simulated sun light with an intensity of 100 mW cm^{-2}. The current density (J)–voltage (V) curve of cell underactive area of 0.23 cm^2 was recorded by using Gamry 1000 interface measurement
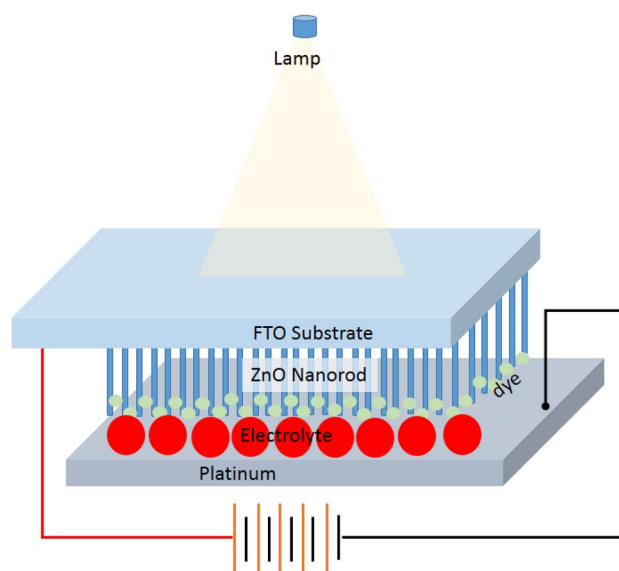
Fig. 1 The DSSC cell with ZnONRs/electrolyte/platinum structure

unit. Meanwhile, the X-Ray diffraction (XRD), Halo DB-20 UV–Vis spectrometer, and Carl Zeiss Supra 55VP field emission scanning electron microscopy (FESEM) were used to investigate the composite structure, optical absorbance properties, and morphology of the sample.

3 Result and discussion

The crystal structures of the samples were characterizedusing Bruker D8 Advanced X-ray diffractometer with CuKα irradiation operated at a scan rate of 0.025°/0.1 s. The XRD spectra of the nanorod grown using various precursor concentrations (K0.02, K0.03, K0.04, K0.05, and K0.06) are shown in Fig. 2. There are four XRD peaks detected from the sample,of which can be associated with the hexagonal wurtzite structure of ZnO (JCPDS card no. 36-1451) with the diffraction peaks at position of 2θ = 31.9°, 34.4°, 36.48° and 2θ = 47.75° correspond to the diffraction from the crystal plane of (100), (002), (101) and (102), respectively. As can be seen from the figure, the diffraction intensity from the crystalline plane of (002) is much higher compared to others crystal plane. This reflects that this crystal plane mainly oriented parallel to the substrate, rendering the nanorod growth are oriented on that plane, which is in good agreement with the previous report [2, 26]. Thus, the crystal plane of (002) is oriented perpendicular to the direction of the c-axis [27]. In addition, in the sample of K0.02, K0.03 and K0.05, it is also detected a weak peak at 2θ = 38°, which is believed to be from the FTO substrate. The second highest diffraction peaks is from the crystal plane of (101). The ratio of the

Fig. 2 The XRD spectra of ZnONRs at various condition of PC
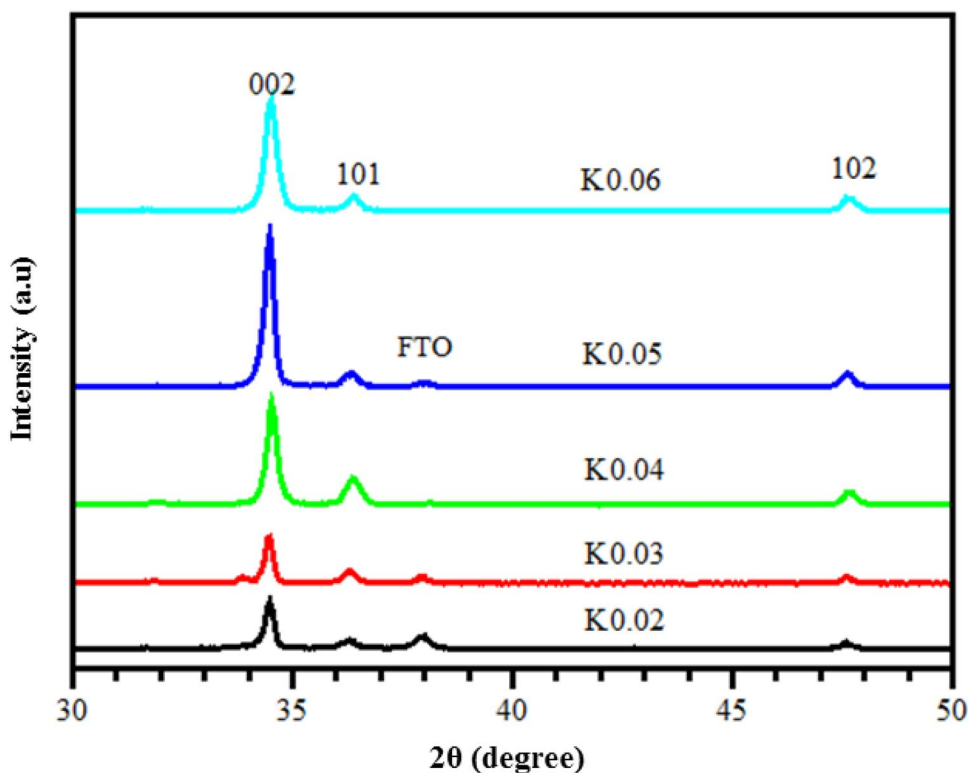
peak height of the plane (002) to the plane (101) increase as the PC increased. The optimum ratio was achieved on the sample of K0.04. However, the ratio decreases when the PC concentration further augmented (K0.05) due to low-density of nanorod growth as the result of high steric hindrance at high PC concentration.

At high concentrations, the formed Zn^{2+} and OH^- ions are believed to dominantly promote to the growth of growing ZnONRs, instead of promoting others nanoseed on the substrate surface. As a result, there is some area of substrate that is not coverage by ZnONRs. When excessive PC concentration is further available in the reaction, for example in the case of sample K0.06, the formed zinc and hydroxyl ions, beside promoting the nanorod's height growth they also accelerate the lateral growth of the nanorods, producing larger diameter nanorod on the surface [28]. Owing to the availability of un-coverage surface, lower X-ray diffraction intensity from this plane is expected.

During ZnONRs growth proces, there are two major components that play an important role i.e. zinc nitrate hexahydrate and hexamethylenetetramine (HMT), which form tetrahedral $[Zn(OH)_4]^{2-}$ or $[Zn(NH_3)]^{2+}$ complexes [29, 30]. This complex will be hydrolized forming chemically un-stable ZnO_4 complex, which then will be dissociated,promoting the growth of ZnO nanocrystals. In the presence of unique polymorphism of hexagonal wurtzite structure [31, 32], the nanocrystal growth of ZnO oxide will possess dominant (002) crystal plane [28].

The morphology of ZnONRs grown on the FTO substrate that are prepared using various PC are examined using FESEM analysis (see Fig. 3). As the Fig. 3a reveals, for the samples prepared at low PC (K0.02), it can be seen that the average diameter and height of ZnONRs is 43 and 283 nm, respectively. Meanwhile the average growth's orientation of the rod normal to the substrate surface is 10.9°. This shows that the ZnONRs growth for this PC is somewhat rare and still have the surface,which is not overgrown by nanorod. Due to such condition, the ZnONRs growth seems skewed with the average density of 136 rod/μm^2.

By increasing the PC (see Fig. 3b–d), the diameter and height of ZnONRs increased. While the average slope decreased with the increasing of PC and maximum at sample K0.05 (see Table 1, Fig. 4). This could be due to the increasing of the diameter of nanorods, resulting in the enhancement of inter-rods coupling supporting well-vertical aligned ZnONRs growth on the substrate. At high of PC, i.e. samples of K0.05 and K0.06 (see Fig. 3d, e), most of the nanorod diameter are higher than 100 nm. Therefore, considering the nanoregime is in between of 1-100 nm, the optimum PC for well-aligned ZnONRs growth is K0.04.

Futhermore, the nanorod density, which is determined by the number of nanorod growth over the substrate area, shows increasing with the increasing of PC and optimum on the sample K0.04. When the PC further augmented, the density significantly decrease as the result of nanorod diameter increasing. From the Table 1, it can be seen that
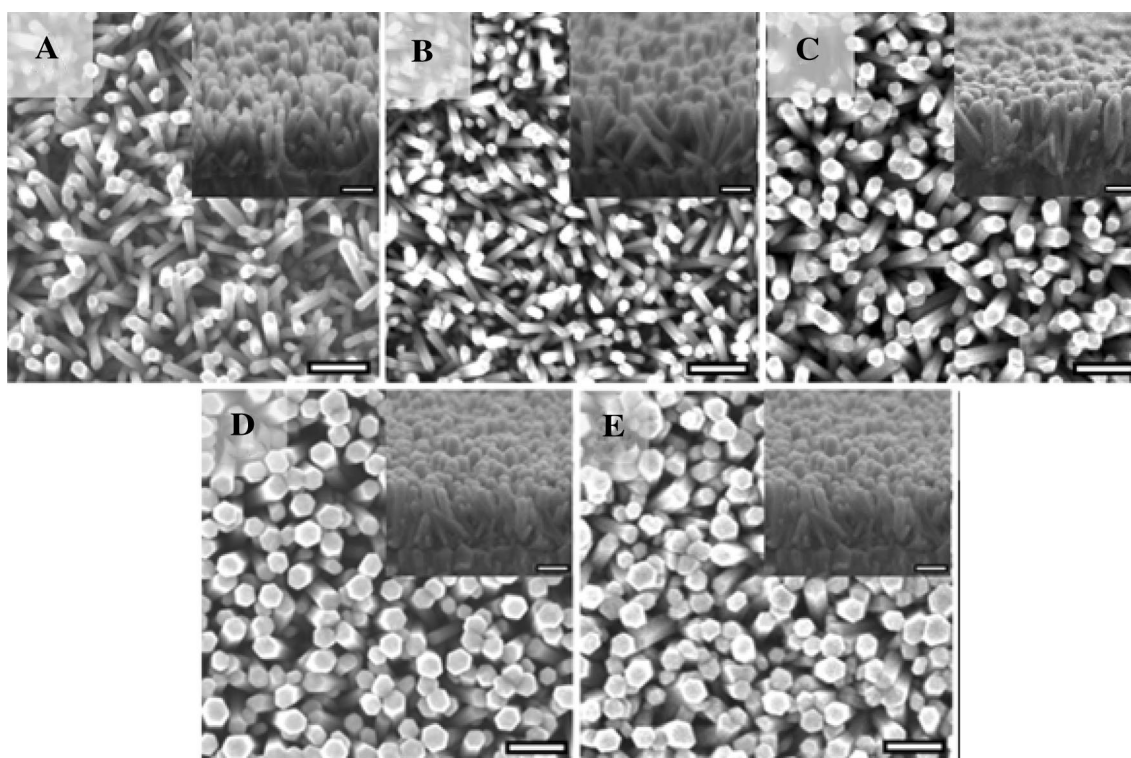
Fig. 3 **a–e** are the FESEM image of ZnONRs grown at various concentration of PC, i.e. 0.02–0.06 M. The *inset* figure is the cross-sectional image of corresponding ZnONRs

Table 1 The diameter, height, slope, and density data of ZnONRs at various PC

Sample	The average of diameter (nm)	The average of height (nm)	The average of slope (degree)	Density (number/ μm^2)
K0.02	43.47 ± 4.7	283.27 ± 47	10.9 ± 1.5	136
K0.03	44.44 ± 5.5	298.18 ± 49	9.7 ± 1.4	144
K0.04	64.14 ± 8.3	363.72 ± 34	6.0 ± 1.0	182
K0.05	86.50 ± 9.8	498.72 ± 116	3.4 ± 2.2	121
K0.06	87.82 ± 7.5	336.81 ± 41	6.8 ± 1.1	106

(based on the diameter, height, slope and density) the well-aligned ZnONRs was achieved at the sample of K0.04. This is in good agreement with the XRD results.

The optical absorption properties of ZnONRs was examined via UV–VIS spectroscopy in the wavelength range of 300–600 nm (see Fig. 5). From the figure it can be seen that the entire samples of ZnONRs exhibit an absorption band centering at 367 nm. This is equivalent to optical band gap energy of ZnO, i.e. 3.37 eV. It can also be seen that the absorbance of the sample increases with the increasing of PC. This is due to the increasing in the diameter and height of the nanorod as well as the surface area [33]. This condition would be beneficial for adsorption of much dye when being used as photoanode of

DSSC, improving the power conversion efficiency (PCE) [34, 35] (see Fig. 6).

We then applied the samples as photoanode in dye-sensitized solar cells. Figure 6 shows the current density–voltage (J–V) curve of DSSC utilizing ZnONRs as photoanode, N719 dye, iodie/triiodide electrolyte and platinum counter electrode in the dark and under illumination of a simulated AM 1.5 G sunlight at 100 mW/cm². The photovoltaic parameter of the DSSC device are summarized in Table 2. As can be seen from the figure, the J-V curve characteristic under the light illumination indicate a significant change in the current flow direction, i.e. changes from positif to negative direction when being illuminated by the light source, reflecting the photovoltaic properties. As also can be seen from the figure, the current density increases with the increasing of PC and optimum at the DSSC device utilizing sample K0.04. This could be due to its high optical absorption. As judged from the FESEM result as shown in Fig. 3c, the sample K0.04 has the highest in the ZnONRs density. This certainly yields a large surface area for dye adsorption or dye loading [34]. This condition may facilitate effective sensitization by the dye molecules, generating a larger photogenerated current density. The best performance DSSC device (i.e. K0.04) produces a short circuit current density, open circuit voltage and PCE as high as 0.86 mA/cm², Voc 0:49 V and 0.16%, respectively. However, in good agreement with the FESEM result, the sample K0.05

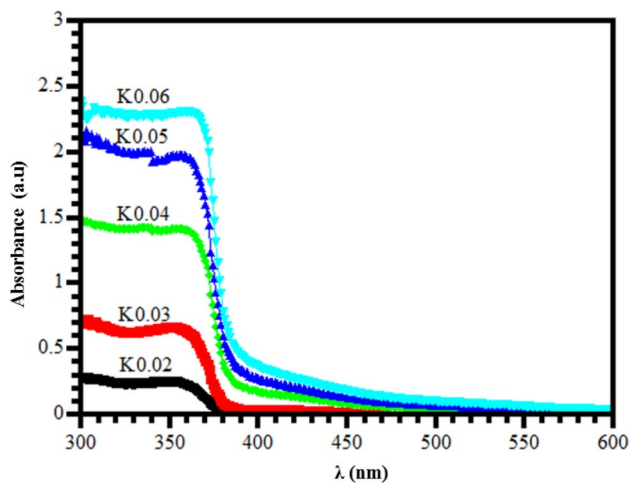**Fig. 4** The diameter, height, slope and density of ZnONRs at various PC condition (K0.02–K0.06)
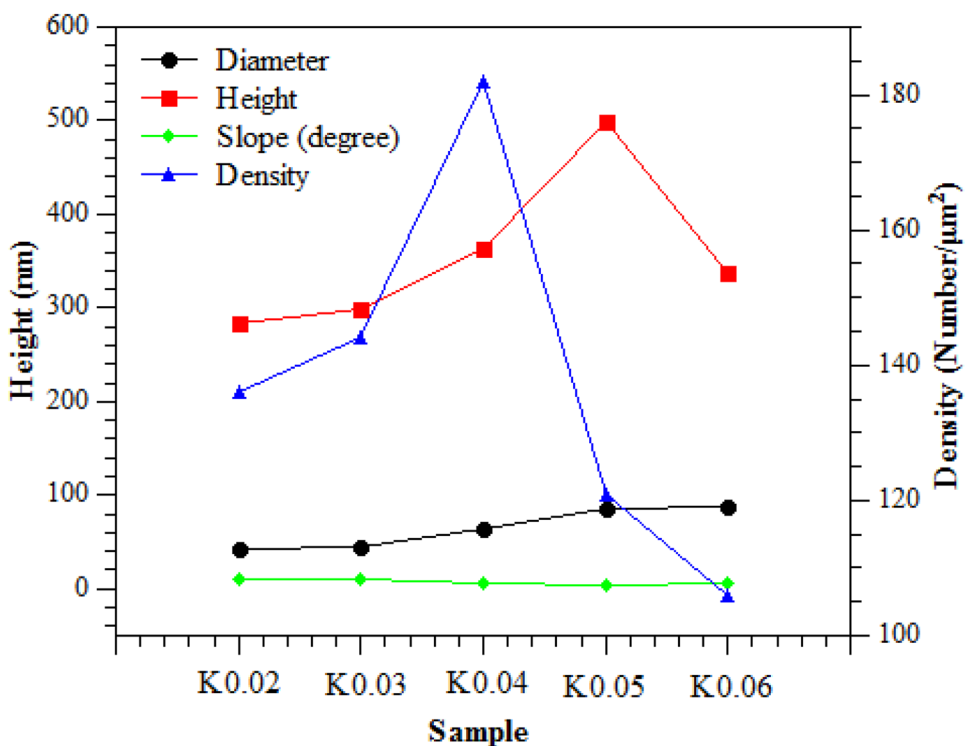

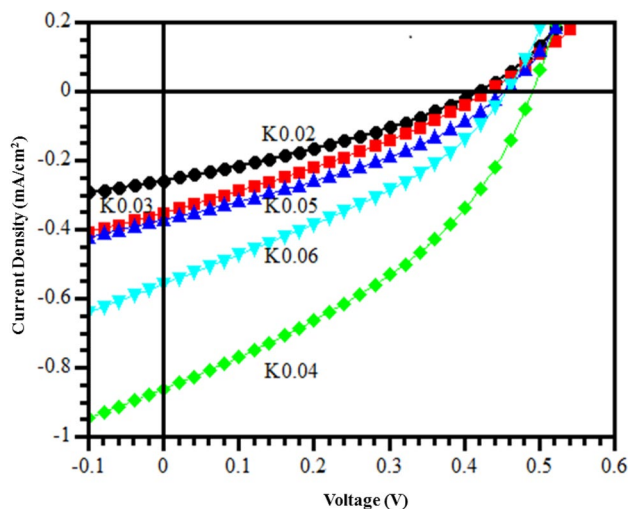**Fig. 5** The optical absorption spectra of ZnONRs at various PC condition (K0.02–K0.06)

Fig. 6 The current–voltage (J–V) characteristics of DSSC cell utilizing ZnONRs at a various PC with platinum as a counter electrode

and K0.06 show lower performance than the sample K0.04. This is presumably attributed to the loss in the quantum effect as the ZnONRs size are larger than 100 nm.

4 Conclusion

The well-aligned ZnONRs arrays on substrate surface has been sucessfully obtained via a hydrothermal process at various PC under 90 °C for an hour of growth time. The

Table 2 The photovoltaic parameter of the DSSCs devices

Sample	Voc (V)	Jsc (mA/cm^2)	PCE (%)	FF (%)
K0.02	0.42	0.26	0.03	0.32
K0.03	0.43	0.36	0.05	0.30
K0.04	0.49	0.86	0.16	0.38
K0.05	0.45	0.37	0.06	0.34
K0.06	0.45	0.56	0.08	0.34

red shifts of the optical absorption band peak confirm the increasing of ZnONRs alignment. The highest nanorod's density of 182 number/μm^{-2}, diameter of 62.96 ± 16 nm, and aligned percentage of $83 \pm 12\%$ (average slope degree of about 6°) was obtained at the sample of K0.04. The best aligned ZnONRs has been used as photoanode in DSSC solar cell devices with a structure of FTO/ZnONRs: dye/electrolyte/platinum/FTO. The optimum device produces a short circuit current density, open circuit voltage and PCE as high as 0.86 mA/cm^2, 0.49 V and 0.16%, respectively.

References

1. G. Amin et al., Influence of pH, precursor concentration, growth time, and temperature on the morphology of ZnO nanostructures grown by the hydrothermal method. J. Nanomater. **2011**, 1–9 (2011)

2. M.G. Ganchenkova, T.T. Vehviläinen, R.M. Nieminen, in *Exotic Carbon Phases: Structure and Properties Computer-Based Modeling of Novel Carbon Systems and Their Properties*, ed. by L. Colombo, A. Fasolino (Springer, New York, 2010). pp. 207–240

3. Z.R. Tian et al., Complex and oriented ZnO nanostructures. Nat. Mater. **2**(12), 821–826 (2003)

4. S. Xu et al., Density-controlled growth of aligned ZnO nanowire arrays by seedless chemical approach on smooth surfaces. J. Mater. Res. **23**(08), 2072–2077 (2008)

5. J. Singh et al., Formation of aligned ZnO nanorods on self-grown ZnO template and its enhanced field emission characteristics. App. Surf. Sci. **256**(21), 6157–6163 (2010)

6. A, A.U., et al., A simple route to vertical array of quasi-1D ZnO nanofilms on FTO surfaces: 1D-crystal growth of nanoseeds under ammonia-assisted hydrolysis process. Nanoscale Res. Lett. **6**. (2012)

7. A. Sobhani, M. Salavati-Niasari, Synthesis and characterization of FeSe 2 nanoparticles and FeSe 2/FeO (OH) nanocomposites by hydrothermal method. J. Alloy Compd. **625**, 26–33 (2015)

8. A. Sobhani, M. Salavati-Niasari, Hydrothermal synthesis, characterization, and magnetic properties of cubic MnSe 2/Se nanocomposites material. J. Alloy Compd. **617**, 93–101 (2014)

9. A. Sobhani, M. Salavati-Niasari, Synthesis and characterization of a nickel selenide series via a hydrothermal process. Superlattice Microstruc. **65**, 79–90 (2014)

10. A. Sobhani, M. Salavati-Niasari, Morphological control of MnSe 2/Se nanocomposites by amount of hydrazine through a hydrothermal process. Mater. Res. Bull. **48**(9), 3204–3210 (2013)

11. A. Sobhani, M. Salavati-Niasari, CdSe nanoparticles: facile hydrothermal synthesis, characterization and optical properties. J. Mater. Sci. **26**(9), 6831–6836 (2015)

12. A. Sobhani, M. Salavati-Niasari, Optimized synthesis of ZnSe nanocrystals by hydrothermal method. J. Mater. Sci **27**(1), 293–303 (2016)

13. A. Sobhani, M. Salavati-Niasari, Hydrothermal synthesis of CoSe nanostructures without using surfactant. J. Mol. Liq. **220**, 334–338 (2016)

14. A. Sobhani, M. Salavati-Niasari, Cobalt selenide nanostructures: Hydrothermal synthesis, considering the magnetic property and effect of the different synthesis conditions. J. Mol. Liq. **219**, 1089–1094 (2016)

15. M. Kashif et al., Sol–gel synthesis of Pd doped ZnO nanorods for room temperature hydrogen sensing applications. Ceram. Int. **39**(6), 6461–6466 (2013)

16. E.L. Lim et al., Enhancement of ZnO nanorod arrays-based inverted type hybrid organic solar cell using spin-coated Eosin-Y. Semicond. Sci. Technol. **28**(4), 045009 (2013)

17. R.T. Ginting et al., MEH-PPV and PCBM solution concentration dependence of inverted-type organic solar cells based on Eosin-Y-coated ZnO nanorod arrays. Int. J. Photoenergy **2013** (2013)

18. R. Taslim et al., Fabrication of Photoelectrochemical cell using highly compact vertical array Zno nanorod. Adv. Mater. Res. **364**, 293–297 (2012)

19. M.I.A. Umar, Effect of growth temperature on ZnO nanorod properties and dye sensitized solar cell performance. KnE Eng. (2016), https://doi.org/10.18502/keg.v1i1.509

20. F.Y. Naumar et al., Polythiopene sodium poly [2-(3-thienyl)-ethoxy-4-buthylsulfonate] inkjet printed film-sensitized ZnO nanorods solar cells. Int. J. Electrochem. Sci. **10**, 445–455 (2015)

21. M.I. Ali Umar et al., Formation of gold-coated multilayer graphene via thermal reduction. Mater. Lett. **106**, 200–203 (2013)

22. M.I. Ali Umar et al., Characterization of multilayer graphene prepared from short-time processed graphite oxide flake. J. Mater. Sci. Mater. Electron. **24**(4), 1282–1286 (2013)

23. M.I.A. Umar et al., Effect of thermal reduction temperature on the optical and electrical properties of multilayer graphene. J. Mater. Sci. **28**(1), 1038–1041 (2017)

24. M.I.A. Umar et al., The effect of spin-coated polyethylene glycol on the electrical and optical properties of graphene film. Appl. Surf. Sci. **313**, 883–887 (2014)

25. M.I.A. Umar et al., Effect of graphite oxide solution concentration on the properties of multilayer graphene. AIP Conference Proceedings. AIP (2013)

26. A. Chrissanthopoulos et al., Synthesis and characterization of ZnO/NiO p–n heterojunctions: ZnO nanorods grown on NiO thin film by thermal evaporation. Photonics Nanostruct. **9**(2), 132–139 (2011)

27. J.Y. Chen, K.W. Sun, Growth of vertically aligned ZnO nanorod arrays as antireflection layer on silicon solar cells. Sol. Energ. Mater. Sol. C **94**(5), 930–934 (2010)

28. F. Ahmed et al., Rapid and cost effective synthesis of ZnO nanorods using microwave irradiation technique. Func. Mater. Lett. **4**(01), 1–5 (2011)

29. A.A. Umar et al., A simple route to vertical array of quasi-1d zno nanofilms on fto surfaces: 1d-crystal growth of nanoseeds under ammonia-assisted hydrolysis process. Nanoscale Res. Lett. **6**, 1–12 (2011)

30. A.A. Umar, M. Oyama, A seed-mediated growth method for vertical array of single-crystalline CuO nanowires on surfaces. Cryst. Growth Des. **7**(12), 2404–2409 (2007)

31. S.T. Tan et al., Formation of a multi-arm branched nanorod of ZnO on the Si surface via a nanoseed-induced polytypic crystal growth using the hydrothermal method. Sci. Adv. Mater. **5**(7), 803–809 (2013)

32. S.T. Tan, A. Ali Umar, M.M. Salleh, (001)-Faceted hexagonal ZnO nanoplate thin film synthesis and the heterogeneous catalytic reduction of 4-nitrophenol characterization. J. Alloy Compd. **650**, 299–304 (2015)

33. S. Javaid et al., Influence of optical band gap and particle size on the catalytic properties of Sm/SnO$_2$-TiO$_2$ nanoparticles. Superlattice Microstruct. **82**, 234–247 (2015)

34. M. Guo et al., The effect of hydrothermal growth temperature on preparation and photoelectrochemical performance of ZnO nanorod array films. J. Solid State Chem. **178**(10), 3210–3215 (2005)

35. M.Y.A. Rahman et al., Effect of organic dye on the performance of dye-sensitized solar cell utilizing TiO2 nanostructure films synthesized via CTAB-assisted liquid phase deposition technique. Rus. J. Electrochem. **50**(11), 1072–1076 (2014)